Proceedings of Montreal 2018
Global Power and Propulsion Forum
7th – 9th May, 2018
www.gpps.global

GPPS-NA-2018-0042

CONVERGENCE CRITERIA FOR AXIAL COMPRESSOR FLOW CALCULATIONS

Andrew A. Vekinis
Whittle Laboratory
University of Cambridge
andrew.vekinis@cantab.net
Cambridge CB3 0DY, England

John P. Longley
Whittle laboratory
University of Cambridge
jpl@eng.cam.ac.uk
Cambridge CB3 0DY, England

ABSTRACT

Computational fluid dynamics is routinely used in the turbomachinery industry to aid in the design of axial flow compressors. The predictive capability of such codes is related to the quality of the numerical convergence of the flow solutions they produce. In certain cases convergence cannot be attained and various publications have linked this to the boundary conditions used within the code. In this paper an investigation in to how common types of boundary conditions affect the numerical convergence is described. The point at which steady-state calculations fail to predict the increasing non-axisymmetric flowfield at off-design, part speed operation is identified.

The analysis of the convergence process is combined with numerical experiments to show that the rate of convergence of steady-state mixing-plane multi-stage axial compressor calculations depends upon the operating point on the pressure-rise versus mass flow rate characteristic. Intrinsically, as the calculated overall characteristic reaches its peak the rate of convergence decreases to zero. Ways to enhance the rate of convergence, for example the technique of adding a downstream nozzle, and conditions under which such techniques are likely to be successful are discussed.

INTRODUCTION

Three-dimensional steady-state RANS codes are industry standard tools for day-to-day multi-stage axial compressor design and are used to predict large portions of compressor performance map. For example, predictions of the working line are typically obtained with steady-state calculations, as the physical flow conditions of axial compressors at such points are also steady (Gallimore, 2012).

Steady-state codes are also used in the design process to predict how axial compressors may behave under off-design flow conditions. The extent to which the flow in such off-design conditions can be assumed steady is unclear. However, low-flow operating points at which steady-state calculations no longer converge are used as a rudimentary prediction of where inherently unsteady compressor operation such as stall and surge may begin (Denton, 2010). This has been referred to as "numerical surge" (Denton, 1992) which is where there is an unrecoverable fall in flow velocity throughout the entire flow domain leading to progressively increasing blade row incidence. An a-priori prediction of this “numerical surge” phenomena would be useful as it could aid in the reduction of computational costs.

To achieve this, it is essential to be able to quantify the rate (or lack thereof) at which a steady-state CFD solution can be obtained. In a general sense, the quantification of numerical convergence rate of steady-state solutions of the Euler and Navier-Stokes equations have been made in previous works (Kreiss, 1987; Nordstrom, 1989), but such calculations were performed on domains that were unrepresentative of turbomachinery environments.

Longley (1993) reviews modelling approaches used to consider axial compressor stability that are affected by the sign of the slope of the pressure rise versus flow coefficient characteristic, namely on the growth of two-dimensional (stall-like) flowfield disturbances with circumferential lengthscales larger than a blade pitch within multistage compressors. The relationship between the magnitude of the slope and the rate of convergence is not considered.

This paper presents an investigation into what determines the point at which steady-state multi-stage CFD codes cease to converge. It also investigates the effects of different CFD techniques, such as multi-grid, which are used to enhance the rate of convergence.

The investigations show that the slope of the pressure-rise versus mass flow rate characteristic has a key role in the convergence rate of steady-state CFD codes, which has not been shown in previous literature. Further, it is demonstrated that axisymmetric, surge-like, flowfield coupling between individual blade rows or different components can be used to assist in the convergence of combined compression systems even when the steady CFD calculations of an individual component would not converge.

METHODOLOGY

Calculations are undertaken using an industry standard CFD code, TBLOCK (Denton, 2009), that is applied to a generic geometry representing the IGV, first and second stages of a multi-stage axial compressor operating at 60% of the design speed. For each of these calculations, the same initial flow conditions are used, so that the development of the flow solution can be compared consistently both on and off the working line. In this way, the behaviour of numerical flowfield transients that are borne out of the inherent inaccuracy of an initial flowfield estimate can be monitored as they are influenced by the boundary conditions within the domain.

In order to understand what aspects within these computational tasks determines the rate at which a calculation will converge (as distinct from being locally stable – which is determined by the local time step) a simplified one-dimensional model of the computational domain and its boundary conditions is developed. This simplified model suggests that it is the slope of the overall compressor pressure-rise versus mass flow rate characteristic which has the major effect on the rate of convergence.

Multi-stage CFD Code

All calculations within this work where performed using TBLOCK which is a structured multi-block RANS finite-volume time-marching code developed by Denton (2009), which can perform both steady-state as well as time-accurate simulations in single precision. In each case studied, wall surfaces are considered adiabatic and rigid. Skin friction coefficients and shear stresses are calculated using wall functions, and all boundary layers that developed in the simulations are considered to be fully turbulent. The turbulence model used for all cases is the mixing length model (Denton, 2009). At the computational domain inlet, fixed stagnation pressure and temperature as well as pitch and yaw angle distributions were specified. At the domain outlet, static pressure was specified at the hub, with its spanwise distribution obtained through simple radial equilibrium. The chosen value of the outlet static pressure determines the operating point on the characteristic. A mixing-plane (MP) approach is used to transfer flux averaged quantities between the stationary and moving frames of reference.

For steady-state calculations, the explicit "SCREE" scheme (Denton, 2002) is used, whereas for the reference time-accurate calculations, to observe the physical propagation of information within the computational domain the dual-time stepping technique is used (Jameson, 1991).

The solver also implements various convergence acceleration methods such as "negative feedback", "local time-stepping" and "multi-grids". Negative feedback is a calculation stabilization technique to account for situations where updates across time-steps within the computational domain may vary greatly across vertices (Denton, 2009). Local time-stepping is when each individual computational cell uses the largest allowable local time-step that is permitted by the constraints of the dimensionless CFL number applied to that cell. Therefore, different parts of the flowfield are integrated forward in time at different rates. Thus flowfield perturbations no longer propagate physically through the domain. Marching of the flow solution forward in this 'pseudo-time' can increase the rate at which convergence is achieved (Pullan, 2012). Multi-grids introduce different levels of grid resolution of the same domain, from coarse to fine. These grids overlap and contribute, in a combined way, to updating the flow solution within each cell in the domain. Due to the larger allowable time-steps used in the coarser grid levels, the overall speed at which information is propagated through the domain is increased, thereby increasing the rate of convergence.

Computational Mesh

The meshing methodology that was employed for all the calculations investigated in this paper is that of a structured H-mesh approach for both the main single-passage blocks that enclose the blade-rows, and gridded hub/tip clearance blocks (with 11 grid-points in the gaps). Triangular trailing edges (cusps) are used for each blade-row to avoid issues with spurious negative loading (Denton, 2010) and the pitchwise grid spacing was also made to be pitchwise uniform at the inlet and outlet boundaries of the blade-row blocks. The inlet boundary is situated 1.2 chord lengths upstream of the IGV leading edge and the outlet boundary is positioned 2 chord lengths downstream of the last blade-rows trailing edge.

A mesh independency study was conducted on a multi-stage axial compressor at blade-speeds and operating conditions that are representative of the calculations undertaken in this paper. The number of grid-points were increased until changes in pressure ratios, mass flow ratios and efficiencies were smaller than 0.5%. As a result, all blade-rows were meshed with 118×95×75 grid-points in the axial, spanwise and pitchwise directions respectively, while the gridded hub/tip clearance blocks contained a corresponding 90×11×20 grid-points. Across the various operating conditions tested with each case study, mean values of $y+$ were approximately 35 on the blade-surfaces and 45 in the regions of the hub and casing, which were deemed suitable for the implementation of wall functions.

The influence of nozzle geometries downstream of the compressor stages are also investigated and use the same number of spanwise and pitchwise grid-points as the blade-rows. The area ratio between the inlet and outlets of the nozzle distinguish whether the flow at the exit of the nozzle will be choked or sub-sonic.

ONE-DIMENSIONAL MODEL OF CONVERGENCE

The motivation for developing a one-dimensional model of the computational domain arose from consideration of how steady-state calculations undergo "numerical surge".

Steady-state calculations are typically performed within single-passage domains, and as a result, there is an enforced circumferential periodicity of the flowfield across all blade-rows. This implies that, any physical flowfield disturbances that may develop at off-design operating conditions in the

single-passages, cannot grow beyond one blade pitch. In the calculations, the behaviour of these physical disturbances (or numerical flowfield transients) may only impact the flowfield in an axisymmetric manner which elucidates the concept of one-dimensional surge-like failure, akin to the "numerical surge" mentioned in the literature (Denton, 1992; Longley, 1994; South, 1997).

The use of mixing-planes in the calculations also impacts how the numerical flowfield transients are communicated between blade-rows. Although mixing-planes generally involve spanwise variations in the flowfield properties, no pitchwise variations can be transferred between adjacent blade rows.

It is hypothesised that the overall numerical convergence of the steady-state calculations is related to the propagation of these one-dimensional (i.e. spanwise and pitchwise uniform) perturbations, exacerbated by the usage of single-passage blade-rows.

Development of the Model

The computational domain can be simplified into a sequence of axisymmetric one-dimensional flowfields, as shown in Fig. 1. The compression system is connected to the inlet and outlet domain boundary conditions by means of computational ducts which can be of arbitrary length. Typically at the inlet boundary a fixed values of stagnation pressure, $p_{0,inlet}$, along with temperature and flow angles are specified. At the outlet boundary the static pressure, p_{outlet}, is specified. Any imbalance between the pressure difference specified by the boundary conditions $(p_{0,inlet} - p_{outlet})$ and the pressure difference across the compressor components $(p_{01} - p_2)$ will cause an acceleration of the flow through the computational domain. It is proposed that this is the basic mechanism which is associated with the axisymmetric, surge-like, convergence failure.

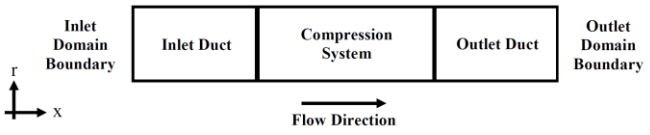

Figure 1: Schematic of the compression system domain and boundary conditions.

In order to encapsulate the above mechanism into a simple model, certain assumptions need to be made. The computational domain is assumed to consist of single-passage geometries of constant streamwise area and the flow is incompressible, axisymmetric with zero inlet swirl angle. Assuming incompressible "slug" flow:

$$\frac{d\phi}{dt} = \frac{(p_{0,inlet} - p_{outlet})}{\rho UL} - \frac{(p_{01} - p_2)}{\rho UL} \qquad (1)$$

where L is the effective length of the domain.

By considering the linearized solutions for unsteady one-dimensional flow in a constant area duct and matching them to the boundary conditions, see Appendix, any axisymmetric perturbation to the flow coefficient will develop in time according to:

$$\delta\phi \propto \exp\left\{\frac{U}{L_1 + L_2}\frac{d\psi^{ts}}{d\phi}t\right\} \qquad (2)$$

A simple one-dimensional mathematical model has been developed to determine how an axisymmetric mass-flow rate disturbance (denoted by the local flow coefficient) present in a calculation would evolve during the process of numerical convergence. It shows that, the rate at which flow disturbances will settle down within the calculation will depend on how negatively sloped the total-to-static pressure rise is. Further, at a computational operating point which has a positively sloped characteristic then, according to equation (2), calculations will undergo a growing and destabilising variation in the mass-flow rate leading to divergence.

It should be noted that the model is suitable only for low-speed calculations due to the assumption of incompressibility discussed earlier. Additionally, the model does not consider cases where stall suppression mechanisms have been implemented.

CONVERGENCE STUDIES

To investigate the convergence of the steady-state CFD code, the computational domain used is the first three blades rows, *IGV+stage1*, of the generic multistage axial-flow compressor. The 3D geometry includes tip gaps, has a single passage per blade row and is calculated using mixing planes.

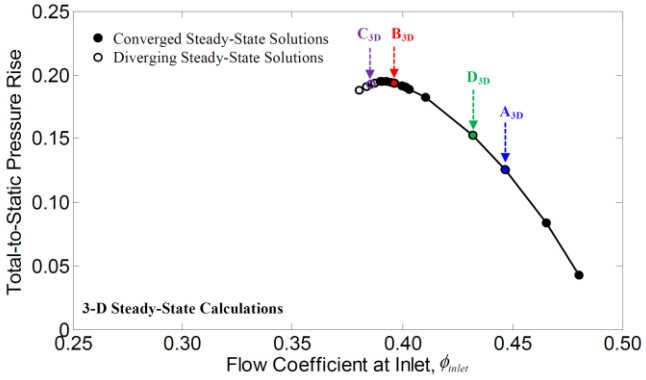

Figure 2: Overall Characteristic for an *IGV+1stage* generic geometry at 60%blade-speed. Operating points of interest are labelled

Convergence limit for a Steady-State Calculation

For the *IGV+stage1* operating at 60% of the design speed the calculated total-to-static pressure rise for a range of inlet flow coefficients is shown in Fig. 2. All the calculations had at least 60×10^3 iterations. The operating points which converged, and could be run for further iterations without change, are denoted by solid filled symbols. The open symbols are those calculations which diverged – these will be discussed later.

From Fig. 2 it is clear that for those operating points which converged, the gradient of the overall total-to-static pressure rise characteristic is negative. Further, those

calculations that diverged appear to correspond to operating conditions where the characteristic has a positive slope. These observations are consistent with Eq. (2).

Rate of Convergence

The rate of numerical convergence can be observed by monitoring for each iteration the mass flow rate at the inlet boundary to the computational domain. The mass flow rate is a useful convergence metric as it is easily determined and it influences all other flow properties within the solution. Other convergence metrics such as percentage changes of flow property residuals within cells typically used in convergence histories are not used due to the difficulty of identifying convergence of the overall domain.

In Fig. 2, three filled (converged) and one hollow (diverging) operating points have been colour coded to aid with the analysis of the convergence data.

The variation in the inlet mass flow rate during the calculations for operating points A_{3D} and B_{3D} are shown in Fig. 3. Note that $\delta\dot{m}$ is the absolute difference between the mass flow rate at iteration N and the converged value. Both calculations converge to about $\ln(\delta\dot{m}) \sim -7$ where the code reaches the limits of numerical precision. Lines have been added to identify the regions of (largely) monotonic convergence.

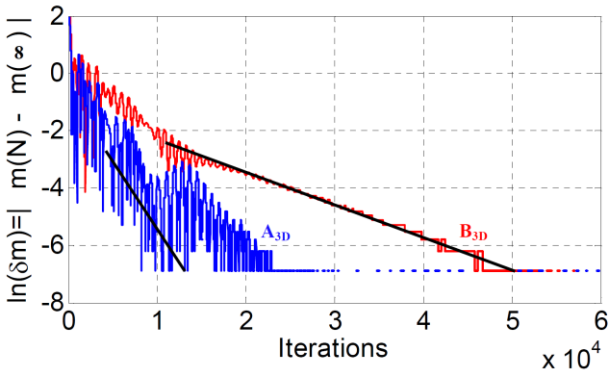

Figure 3: Variation of inlet mass flow rate against iteration number for converged calculations A_{3D} and B_{3D} (at 60% blade-speed).

Considering the y-axis on Fig. 3, for the calculation corresponding to operating point A_{3D}, $\ln(\delta\dot{m})$ changes by -4.81 during 10×10^3 iterations whilst for B_{3D}, $\ln(\delta\dot{m})$ changes by only -1.04 during 10×10^3 iterations. The calculation for operating point B_{3D}, which is almost at the peak of the calculated total-to-static pressure rise characteristic, takes approximate five times as many iterations to converge than that for A_{3D} which is at a lower pressure rise and higher mass flow rate.

It should be noted that for both operating points there is an initial grouping of two oscillations in $\ln(\delta\dot{m})$, across the first 20×10^3 iterations. For operating point B_{3D}, this is less pronounced (as compared to A_{3D}) as in this case, oscillations in the mass flow during convergence are lower than the changes in the overall mass flow. For the A_{3D} the converged value of the mass flow rate is reached faster.

These observations are in general agreement with Eq. 2 which relates the time development of a flow coefficient perturbation to the slope of the total-to-static pressure rise characteristic. At operating point A_{3D} the characteristic has a large negative slope whilst at operating point B_{3D} there is only a small negative slope.

Convergence Rate and Slope of Characteristic

For a comparison between the model, Eq. 2, and the observed convergence behaviour of the steady-state CFD code it is necessary to define the *convergence rate* Θ by:

$$\delta\dot{m} \propto e^{\Theta N} \tag{3}$$

This is consistent with the values determined from Fig. 3.

Comparing Eqs 2 and 3, noting that $\delta\dot{m} \propto \delta\phi$ and that the number of iterations N is (approximately) related to the simulation time, since the "SCREE" scheme uses explicit time-stepping, then the convergence rate:

$$\Theta \sim \frac{U}{L_1 + L_2}\frac{d\psi^{ts}}{d\phi} \tag{4}$$

If the numerical scheme that is used was implicit, then the relation between iteration number and simulation time would not hold since in an implicit solver the closer the calculation is to a steady-state solution the faster it is reached.

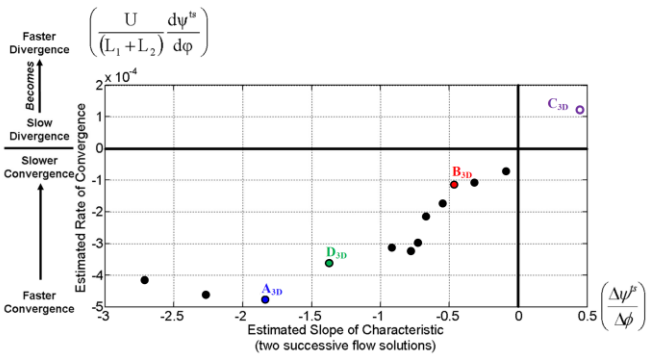

Figure 4: Relationship of convergence rate with the slope of the performance characteristic for the operating points of Fig. 2.

For the calculations shown in Fig. 2 the convergence rate is compared with the slope of the total-to-static pressure rise characteristic in Fig. 4. (The slope is estimated from two adjacent operating points.)

Figure 4 shows that there is a relationship between the convergence rate of the calculation and the slope of the total-to-static pressure rise versus flow coefficient characteristic. This is in agreement with Eq. 2. Further, for the converged solutions the convergence rate, Θ, becomes zero as the slope approaches zero from below. Any operating point, e.g. C_{3D}, which would correspond to a positive slope diverges.

Additionally, using point "A_{3D}" as a comparison, two operating points at more negative slopes have slower convergence rates. At higher flow-rates, flow will approach

the leading edges of the blades at a more negative incidence. This may lead to flow disturbances developing within the computational domain which may excite axisymmetric perturbations which may affect convergence. This observation shows that although the developed model is applicable for specific calculated operating ranges, there might be avenues of improvement.

Converging – Diverging Steady-State Calculations

An aspect that needs to be considered in the context of numerical convergence is the movement of the calculated operating point on the total-to-static pressure rise versus flow coefficient performance map during convergence/divergence. Operating points B_{3D} (converging case) and C_{3D} (diverging case) shown on Fig. 2 are now discussed with the focus on monitoring their movement with iteration number, Fig. 5.

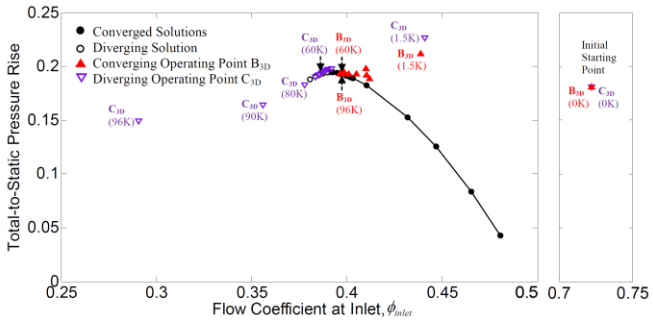

Figure 5: Movement of calculated operating points B_{3D} and C_{3D} with iteration number.

In Fig. 5, all the black operating points on the characteristic have been run for 60×10^3 iterations. The coloured operating points B_{3D} and C_{3D} have been run for 96×10^3 iterations. All the calculations used the same initial conditions with the starting point shown on the extended right side of the graph (same y-axis, different x-axis). The contours of axial Mach number at mid-span in the blade-to-blade view for B_{3D} and C_{3D} are shown in Fig. 6 at 30×10^3, 60×10^3 and 96×10^3 iterations.

It can be observed that for C_{3D} divergence is only apparent for $N > 60\times10^3$ where there is a drop in axial Mach number across the entire domain. The failure of the calculation leads to progressively increasing incidence on the first rotor (R1), flow separation and deviation at the exit of the first stator (S1) and consequently increased loss. In contrast, the converging operating point B_{3D}, has no change.

The lack of convergence for the C_{3D} calculation could easily be missed if less than 60×10^3 iterations had been used. Although the diverging solution is not reliable, it may, however, suggest areas within the domain that could be worthy of further aerodynamic investigation.

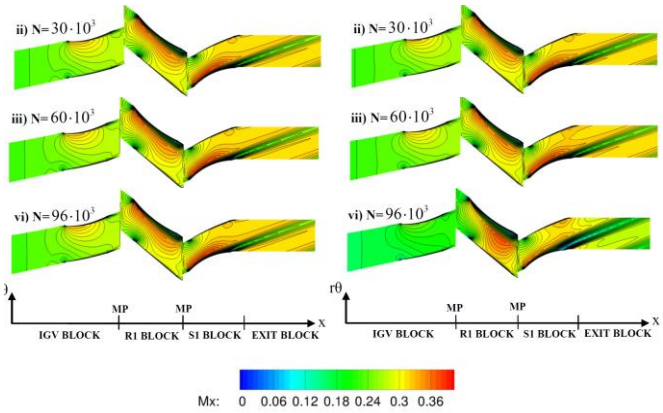

Figures 6: Blade-to-blade mid-span contours of axial Mach number for operating points B_{3D} (left) and C_{3D} (right) with increasing iteration number.

CONVERGENCE ACCELERATION TECHNIQUES

The calculations for all of the operating points in Fig. 2 were undertaken using multi-grids, local time-stepping and the default negative feedback, NF10, (larger numbers after NF correspond to reducing the allowable change in flow properties in any time-step that can occur within the vertices of a single cell). Two of these operating points, A_{3D} and D_{3D}, will now be re-calculated with several of the convergence acceleration techniques disabled and the results are shown in Fig. 7. None of the acceleration techniques affected the converged solutions, so the estimated slopes are unchanged, but disabling the multi-grids and local time-stepping reduced the rate of convergence by approximately a factor of five.

To quantify these effects, and thereby demonstrate that both operating points A_{3D} and D_{3D} are affected similarly, the Convergence Rate Ratio, CRR, will be defined by:

$$\mathrm{CRR} = \frac{\Theta_{\mathrm{A3D}}}{\Theta_{\mathrm{A3D,no\text{-}LT\text{-}MG}}} \qquad (5)$$

where Θ_{A3D} is the convergence rate for A_{3D} with NF10, MG and LT (i.e. as used in earlier calculations) and $\Theta_{\mathrm{A3D,no\text{-}LT\text{-}MG}}$ is the convergence rate when local time-stepping and multi-grid are disabled. The values for the Convergence Rate Ratio are listed in Table 1. Although there are differences between the CRR values for the two operating points they are small compared to the changes caused by disabling the convergence acceleration techniques.

Type of Calculation	A3D	D3D
All enabled with default NF10	1.000	1.000
NF25	0.704	0.791
NF50	0.640	0.712
No local time-stepping	0.439	0.511
No multi-grids	0.237	0.255
No multi-grids, no local time-stepping	0.123	0.139

Table 1: Influence of acceleration techniques on Convergence Rate Ratio for points A_{3D} and D_{3D}.

In Table 1 it can be seen, for example, that removing multi-grids decreases the convergence rate by up to 76.3% whereas an increase of NF10 to NF25 decreases the convergence rate only by 29.6%. It is appreciated that the values of CRR in Table 1 are applicable only for the SCREE numerical scheme that is used for these calculations.

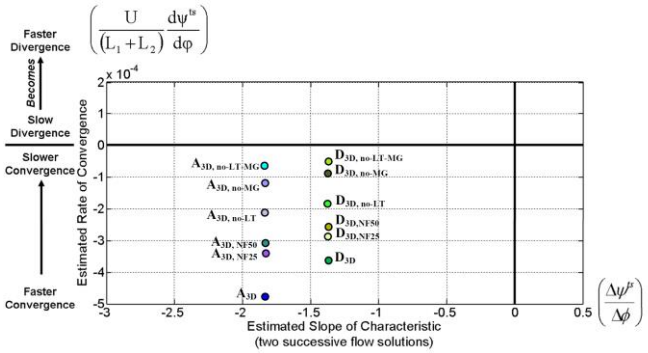

Figure 7: Convergence acceleration techniques and convergence rate for two operating points with different slopes on the performance characteristic.

STEADY-STATE AND TIME RESOLVED METHODS

The studies on the convergence rate of the steady-state calculations have all been performed with the explicit "SCREE" scheme. Because of the convergence acceleration techniques that are employed within the steady-state code, it is valuable to investigate how the non-physical propagation of information within the computational domain affects the rate of convergence. This will be undertaken by comparing against a time-accurate numerical scheme that employs a uniform time-step across the entire domain.

Time-accurate calculations are computationally much more expensive so only a two-dimensional mid-span section of the *IGV+stage1* studied previously will be investigated. The steady-state calculations were undertaken using mixing planes between the blade rows. For the time-accurate calculations both mixing planes and sliding planes will be investigated. The calculated operating points at 60% of design speed are shown in Fig. 8.

Before undertaking the two-dimensional time-accurate calculations, the 2-D mid-span geometry was calculated using the steady-state SCREE solver (used for Fig. 2, including multi-grid, local time-stepping and default negative feedback) to determine the characteristic. For the steady-state SCREE calculations both the converged operating points (black filled squares) and the diverging operating points (black hollow squares) are shown in Fig. 8. As was observed earlier, only the operating points corresponding to a negatively sloping characteristic converged.

The time-accurate calculations were undertaken at two operating points ($A_{U\text{-}2D}$, $B_{U\text{-}2D}$ with MP=Mixing Planes and SP=Sliding Planes), Fig. 8. These two operating points were also repeated ($A_{2D,no\text{-}LT\text{-}MG}$ and $B_{2D,no\text{-}LT\text{-}MG}$) using the steady-state SCREE scheme but with the convergence acceleration methods disabled and a uniform time-step which matched that used in the time-accurate calculations.

On Fig. 8 the steady-state A_{2D} and time-accurate $A_{U\text{-}2D}$ operating points are similar. However, the corresponding B_{2D} and $B_{U\text{-}2D}$ operating points are spread further apart. This is because at off-design points close to the characteristic peak the conditions within the blade-rows are more conducive to developing flow separations. These can affect how the blade rows interact with each other dynamically. Sliding planes can capture more of these interactions than mixing planes thus producing the small differences in the flow solution.

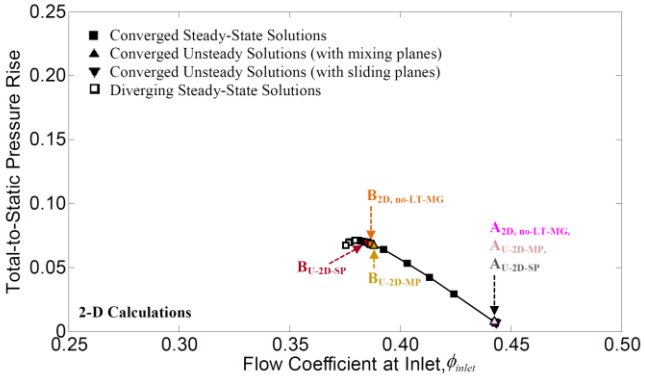

Figure 8: Overall Characteristic for the 2-D mid-span section of the *IGV+stage1* geometry.

Steady-state and time-accurate Convergence rates

In the time-accurate calculations $\delta\dot{m}$ did not tend to zero but reached a limit-cycle due to the unsteady aerodynamic phenomena taking place within the domain. The point at which this occurred marked the point at which the time-accurate solution was considered converged. The convergence rate, Θ, for both the steady-state and time-accurate calculations was evaluated only across iterations for which there was a monotonic decrease in $\delta\dot{m}$.

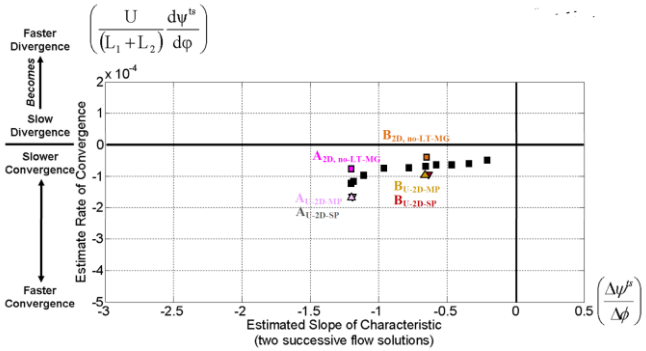

Figure 9: Convergence rate plotted against slope for the 2-D calculations shown in Fig. 8.

For the operating points in Fig. 8 the convergence rates are shown in Fig. 9 plotted against the estimated slope. For the time-accurate operating points $A_{U\text{-}2D}$ and $B_{U\text{-}2D}$ the mixing plane and sliding plane calculations have similar convergence rates because the same uniform time-step is used. The steady-state operating points ($A_{2D,no\text{-}LT\text{-}MG}$ and

$B_{2D,no\text{-}LT\text{-}MG}$) using the steady-state SCREE scheme with the convergence acceleration techniques disabled and with the same uniform time-step converged approximately 2.2 times slower than the time-accurate calculations using Jamesons' dual-time stepping scheme.

When the steady-state SCREE solver was applied to the 2-D mid-span section the convergence rate was between that of the time-accurate 2-D calculations and those where the convergence acceleration techniques had been disabled. However, the convergence rate of the steady-state SCREE solver applied to the 2-D mid-span section was much lower than when it was applies to the full-span 3-D geometry, see Fig. 4. This is because the small spanwise extend of the cells when the steady-state SCREE solver was applied to the 2-D geometry dominated the local time step.

The time-accurate calculations converged at a faster rate than the corresponding steady-state SCREE calculations (convergence acceleration techniques disabled and using the same uniform time-step). This illustrates how the emulation of the physical propagation of flow information in the steady-state calculations differs from the actual physical propagation of flow information in the time-accurate calculations.

COMPONENT COUPLING

The model based on the one-dimensional propagation of axisymmetric perturbations, supported by the numerical investigations, has shown that the rate of convergence is related to the slope of the overall total-to-static pressure rise characteristic. This suggests that as long as convergence is controlled by the one-dimensional disturbances, it ought to be possible to use component coupling to affect the convergence of the flow fields of individual components.

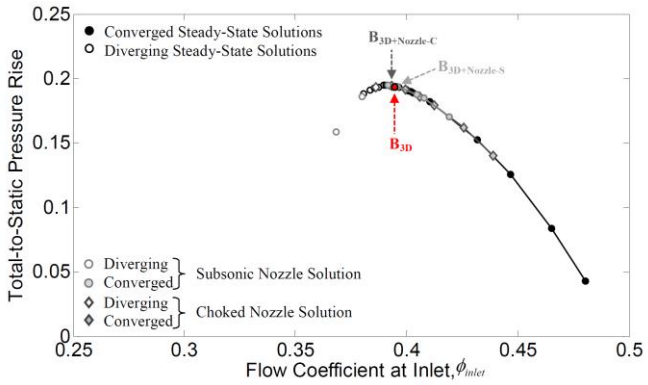

Figure 10: Overall Characteristics for the 3-D geometry *IGV+stage1* operating points with nozzle cases downstream of compression system.

Subsonic and Choked Exit Nozzles

A convergent nozzle has a negatively sloped total-to-static pressure rise characteristic. Therefore placing one upstream of the exit boundary condition, ought to affect the convergence rate of the upstream components. Effectively, the exit static pressure becomes a negatively sloped function of flow coefficient and this ought to affect the convergence rate of the overall computational domain. Figure 10 shows a number of nozzle calculations superimposed onto the 3-D steady-state *IGV+stage1* calculations of Fig. 2. The corresponding mid-span blade-to-blade axial Mach number contours are shown in Fig. 11. The variation in the inlet mass-flow for each of the cases is shown in Fig. 12.

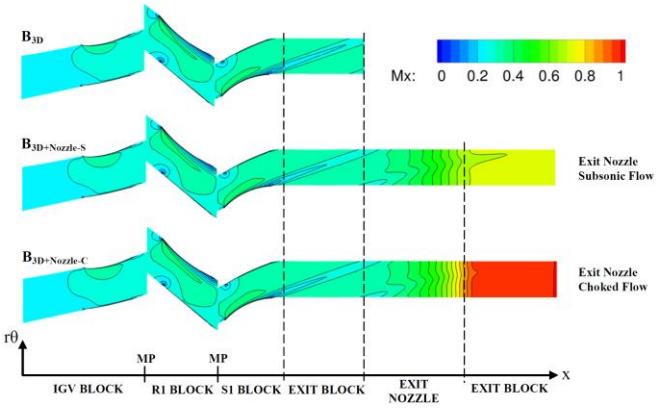

Figure 11: Mid-span blade-to-blade axial Mach number contours for the B_{3D} steady-state operating points shown in Fig. 10.

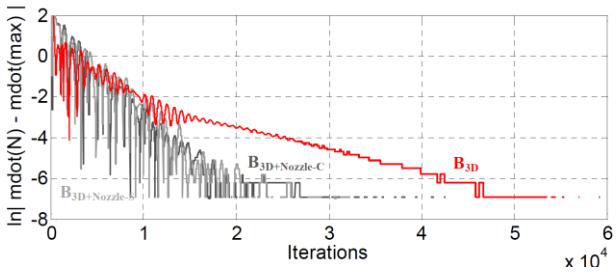

Figure 12: Variation of inlet mass flow in against iteration number for nozzle and non-nozzle operating points in Fig. 10.

Figure 10 shows that each of the B_{3D} operating points are near the peak of the performance characteristic. The slight differences in the values of flow-coefficient and pressure rise is due to entropy being generated by the boundary layers and shock in the choked nozzle.

It should be noted that, for the *IGV+stage1* geometry studied, none of the earlier calculations were able to obtain a converged solution at flow coefficients lower than B_{3D}.

Figure 11 shows the blade-to-blade axial Mach number for each of the calculations. The flowfield is identical within the compression system for each case as the nozzle area-ratios for both the subsonic and choked nozzle have been chosen to ensure this.

Figure 12 shows that the number of iterations required for one order of magnitude drop in the variation in mass flow for both the "$B_{3D+Nozzle\text{-}S}$" and "$B_{3D+Nozzle\text{-}C}$" cases were found to be about ~3.6 and ~3.3 times less respectively than that of case "B_{3D}", without the nozzle. It general, it is observed that the nozzle has a beneficial effect on the convergence rate of the simulation and may permit lower flow coefficients.

The difference in the convergence rates for the subsonic and choked nozzles themselves is related to how information is allowed to propagate across the nozzle. For the subsonic nozzle, flow information can propagate from both inlet and outlet domain boundaries into the interior flowfield. In choked nozzle case however, flow information cannot travel upstream from the exit boundary once the flow has choked.

Coupling between Adjacent Stages

In steady-state calculations adjacent stages are coupled through the interchange of one-dimensional axisymmetric perturbations across the mixing planes. Therefore it is expected that if an additional stage is added downstream of the single stage the convergence rate should be affected. The second stage of the generic multi-stage axial flow compressor will be included in the computational domain to produce the *IGV+2stage* geometry.

The total-to-static pressure rise characteristics for the overall two-stage geometry along with those for the individual first and second stages are shown in Fig. 13. Also included are calculations where a subsonic nozzle was added at the end of the two-stage geometry to investigate whether it would be able to extend the calculations to a lower flow-coefficient convergence limit, ϕ_{CL}. The static pressure value at the exit of the nozzle (outlet domain boundary) was kept constant and the nozzle area-ratio was varied.

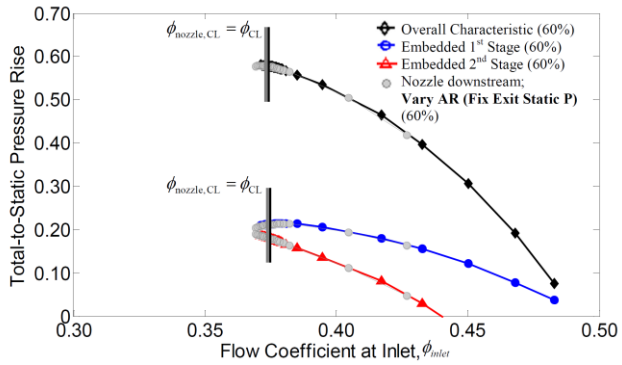

Figure 13: Overall and embedded Characteristics for the *IGV+2Stage* geometry. Calculations with downstream nozzles are also included. Convergence limits are indicated on graph.

In Fig. 13 the vertical black and grey lines denote the convergence limit: calculations at a higher flow coefficient converged whilst those at lower flow coefficients ultimately diverged. This numerical convergence limit will be referred to as ϕ_{CL} and was found to be at a negative slope rather than the peak of the total-to-static pressure rise characteristic. However it was identified that the failure of the calculations was due to reversed flow starting to appear at the inlet of the stator 1 blade row in the casing region. Such flow field disturbances do not couple across the mixing planes so neither a downstream stage nor a downstream nozzle can affect the convergence.

Another observation is that converged operating points can be found on the positive slope for the first stage (embedded within the multi-stage geometry). This is due to the stabilising properties that a downstream stage can have on an upstream one. This observation is in line with the physical effect that downstream stages have on upstream stages as reported in the literature [Longley and Hynes, 1990]. Thus, the conclusion of negative slope convergence stands as long as the gradient of the characteristic is thought of in an overall sense, across the entire computational domain.

DISCUSSION

To deal with the axisymmetric 'surge-like' steady-state flow calculation failure, a novel axisymmetric mathematical model has been developed. It has been shown that, by using the model, the convergence rate can be linked with the slope of the overall performance characteristic. This has important implications that the number of iterations required to obtain convergence of a multi-stage compressor calculations will depend upon the operating point. Operating points near the peak of overall performance characteristics will require a larger number of iterations compared to higher flow-rate operating points to achieve similar levels of convergence. This observation is not expected to apply to multi-stage axial flow turbines because the slope of their performance characteristic do not vary greatly with operating point.

An important point to consider is the influence that the turbulence model can have on the development of large flow separations across blade rows within the domain (Denton, 2010). The presence of a large flow separation will increase deviation and blockage within the passage and the resulting loss will decrease the calculated pressure rise at given instances in the calculation, as shown in Fig. 6. If the flow separation grows to such an extent that the slope of the overall pressure rise versus flow coefficient characteristic has a positive slope (effectively the operating point moves across the peak of the characteristic) then the rate of growth would be expected to accelerate and the solution diverge. In real turbomachines the flowfield may develop rotating stall which cannot be captured in a single passage calculations. Multi-passage time accurate solvers would therefore be expected to develop time varying solutions which steady-state single passage calculations cannot capture. However, the divergence of the steady-state single passage calculations may suggest that an axisymmetric solution does not exist.

The analytical model does not take localised issues such as reversed flows near mixing planes into account and, formally, is only applicable to low-speed calculations where stall suppression mechanisms have not been implemented.

The effect that convergence acceleration methods have on the convergence rate was also investigated with the analytical model. It was found that multi-grids have a greater effect on the convergence rate than local time-stepping methods and negative feedback methods. This leads to an enhancement of the model through the inclusion of a 'Convergence Rate Ratio' term.

The steady-state convergence rate investigations were also compared against benchmark time-accurate calculations. To save computational resources this was done for a two-

dimensional mid-span section of a single-stage geometry. In this study, the steady-state calculations were run in a 'time-accurate' mode by removing both multi-grid and local time-stepping methods in these calculations. It was found using the analytical model, while similar time-steps were ensured for both steady and time-accurate cases, that the numerical scheme which was used for the physical propagation of flow information through the domain in the time-accurate calculations would converge at a rate that was about 2.2 times faster than the steady-state numerical scheme.

The model also shows that downstream components such as subsonic and choked nozzles (which always operate on a negative slope) can increase the convergence rate of axial compressor flow calculations, with the former being marginally more effective. It should be noted that choked nozzles with a specified area ratio act as an exit mass flow boundary condition. However, nozzles cannot affect the non-uniformity of relative stagnation pressure and temperature at the inflow of the Mixing Planes, nor the part-pitch flow reversals that may develop near them.

The novel axisymmetric mathematical model could be used to estimate the rate of convergence based on earlier calculations combined with information regarding the current calculation (thereby allowing an estimate of the effective slope). It could therefore be used to estimate the number of iterations that would be required to achieve a desired level of convergence or to indicate the likely divergence (failure) of the current operating point.

CONCLUSIONS

In the one-dimensional, axisymmetric sense, the cause for surge-like solution failure has been established.

(1) The novel axisymmetric mathematical model has showed that the slope of the overall total-to-static pressure rise versus flow coefficient characteristic is a significant factor in determining convergence: the more negative the slope the greater the rate of convergence.

(2) The multi-grid convergence acceleration technique used in multi-stage CFD codes have the largest effect on the convergence rate followed by local time-stepping methods and finally negative feedback techniques.

(3) The impact of the numerical scheme on the convergence rate was investigated and it was found that Jamesons' dual-time stepping scheme is about ~2.2 faster than the SCREE scheme when run with uniform time-steps.

(4) The addition of adjacent stages with a strong negative slope or a downstream nozzle has been shown to increase the convergence rate.

(5) Neither adjacent stages nor nozzles can influence the interior flow of blade rows such as pitchwise variations (reversed flow) that could develop in the proximity of the mixing planes.

NOMENCLATURE

A	Duct Area [m^2]
b, d	Amplitudes of axisymmetric flow perturbations
i	Imaginary unit
L	Duct Length [m]
M_x	Axial Mach number
$\dot{m}$	Mass flow-rate [kg/s]
N	Iteration number
p	Pressure [Pa]
t	Time [s]
U	Blade-speed
V_x	Axial Velocity [m/s]
x	Axial distance [m]
δq	Small variation of quantity
Θ	Convergence rate
ρ	Density
ϕ	Flow coefficient
ψ^{ts}	Total-to-static pressure rise
ω	Frequency of harmonic oscillation
$\bar{q}$	Mean value of quantity *q*

Sub-scripts and Abbreviations

0	Stagnation
1, 2	Inlet, Outlet Stations
CFD	Computational Fluid Dynamics
CL	Convergence Limit
CRR	Convergence Rate Ratio
IGV	Inlet Guide Vane
inlet	Domain Inlet
MP, SP	Mixing Plane, Sliding Plane
outlet	Domain Outlet

ACKNOWLEDGMENTS

The authors would like to acknowledge the generous funding and support from Siemens Industrial Turbo Machinery Ltd, especially Roger Wells. Thanks are due to Prof. John Denton for the provision of the multi-stage code the forms the basis of all work conducted within this paper. Thanks are also due to Mehdi Vahdati of Imperial College London and Liping Xu of the Whittle Laboratory, University of Cambridge, for their interest and stimulating discussions in regards to the work.

REFERENCES

Denton J.D., 1992, "Calculation of 3D viscous flow through multistage turbomachines", ASME J. Turbomach., **114**(1).

Denton J.D., 2002**,** "The Effects of Lean and Sweep on Transonic Fan Performance: A Computational Study", TASK Quarterly, Vol. 6, No 1, Pages 7-23.

Denton J.D., 2009, "TBLOCK Description and User Manual: Version TBLOCK-09.5 (dated 4/11/2009)", CFD Program Manual.

Denton J.D., 2010, "Some Limitations of Turbomachinery CFD", Proceedings of ASME Turbo Expo 2010: Power for Land, Sea and Air.

Gallimore S.J., 2012, "Axial Compressor Design", Cambridge Turbomachinery Course Lectures Book 2012, Whittle Laboratory, University of Cambridge.

Jameson A., 1991, "Time dependent calculations using multigrid, with applications to unsteady flows past airfoils and wings", AIAA Paper 91-1596.

Kreiss G., 1987, "Convergence to steady-state solutions of the Euler equations I", BIT Numerical mathematics **28**(1), Pages 144-162.

Longley J.P. and Hynes T.P., 1990, "Stability of Flow through Multistage Axial Compressors", ASME J. Turbomach., 112(1), p. 126.

Longley J.P., 1994, "A Review of Non-Steady Flow Models for Compressor Stability", ASME J. Turbomach., **116**(2), p. 202.

Nordstrom J., 1989, "The Influence of Open Boundary conditions on the Convergence to Steady State for the Navier-Stokes Equations", J. Computational Physics, Vol 85, Pages 210-244.

Pullan G., 2012, "Introduction to Numerical Methods for Predicting Flow in Turbomachines", Cambridge Turbomachinery Course Lectures Book 2012, Whittle Laboratory, University of Cambridge.

South A.H., 1997, "Low flow compressor performance", PhD Thesis, Whittle Laboratory, University of Cambridge.

APPENDIX

A one-dimensional model for a computational domain is shown in Fig. A1. The total-to-static pressure rise of the compressor components is modelled as an actuator disk and the flowfield inertia is either upstream or downstream of the actuator disc.

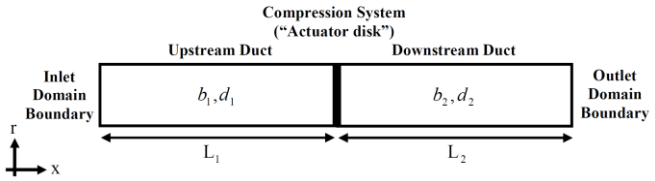

Figure A1: Schematic of domain with compression system modelled as an actuator disk for the analysis of the linearized flow perturbations

For small amplitude one-dimensional incompressible flow perturbations with frequency ω through such a model there are only two types of pressure perturbation:

$$\text{Slug-mode: } \delta p \propto xe^{i\omega t} \qquad \text{Origin-mode: } \delta p \propto e^{i\omega t} \tag{A1}$$

The slug-mode corresponds to pressure varying linearly with distance along the duct and the origin-mode arises depending upon the choice of spatial origin. The form of the perturbation in flow coefficient, pressure and stagnation pressure are given in Table A1.

There are four boundary conditions

$$\delta p_{0,inlet} = 0 \qquad \delta p_{outlet} = 0 \qquad \delta\phi_1 = \delta\phi_2 \tag{A2a}$$

$$\delta\psi^{ts} = \frac{d\psi^{ts}}{d\phi}\delta\phi = \frac{\delta p_2 - \delta p_{01}}{\rho U^2} \tag{A2b}$$

Combining these with the expressions in Table A1 produces, after a little algebra, the following:

$$\frac{d\psi^{ts}}{d\phi} be^{i\omega t} = \left(\frac{iL_1\omega}{U}\right) be^{i\omega t} + \left(\frac{iL_2\omega}{U}\right) be^{i\omega t} \tag{A3}$$

On simplification gives:

$$i\omega = \left(\frac{U}{L_1 + L_2}\right)\frac{d\psi^{ts}}{d\phi} \tag{A4}$$

	$\delta p \propto xe^{i\omega t}$	$\delta p \propto e^{i\omega t}$
Flow coefficient	$\delta\phi = b\mathrm{e}^{\mathrm{i}\,\omega t}$	$\delta\phi = 0$
Static Pressure	$\frac{\delta p}{\rho \mathrm{U}^2} = \left(-\frac{\mathrm{i}\,x\omega}{\mathrm{U}}\right) b\mathrm{e}^{\mathrm{i}\,\omega t}$	$\frac{\delta p}{\rho \mathrm{U}^2} = d\mathrm{e}^{\mathrm{i}\,\omega t}$
Total Pressure	$\frac{\delta p_0}{\rho \mathrm{U}^2} = \left(\bar{\phi} - \frac{\mathrm{i}\,x\omega}{\mathrm{U}}\right) b\mathrm{e}^{\mathrm{i}\,\omega t}$	$\frac{\delta p_0}{\rho \mathrm{U}^2} = d\mathrm{e}^{\mathrm{i}\,\omega t}$

Table A1: Linearized perturbation modes for one-dimensional incompressible flow.